*J. Fluid Mech.* (1988), *vol.* 196, *pp.* 187–204
*Printed in Great Britain*



# Effects of finite depth and current velocity on large amplitude Kelvin–Helmholtz waves

By V. BONTOZOGLOU AND T. J. HANRATTY
Department of Chemical Engineering, University of Illinois at Urbana-Champaign, Urbana, IL 61801, USA

(Received 27 July 1987 and in revised form 7 April 1988)

## 1. Introduction

Over the past decades a large amount of work has been done on inviscid, steady progressive, gravity waves on a free surface. However, waves which occur in nature are never, in fact, free-surface waves, since they are always beneath a fluid of finite density, if only air. In spite of this, very little work has been done on finite-amplitude interfacial waves. Tsuji & Nagata (1973) carried out a perturbation expansion in wave amplitude to fifth order, for interfacial waves between two stationary fluids. Holyer (1979) extended the calculation using the computer and resorted to Pade approximants to sum the resulting series. Meiron & Saffman (1983) investigated numerically the limiting highest wave and demonstrated the existence of overhanging gravity waves of permanent form.

Finite-amplitude interfacial waves between two fluids in relative motion (occasionally called waves with current) have been considered by a number of investigators. Drazin (1970), Maslowe & Kelly (1970), Nayfeh & Saric (1972) and Weissman (1979) developed weakly nonlinear solutions for unbounded fluids. Pullin & Grimshaw (1983*a*, *b*) derived a third-order expansion for arbitrary depths and obtained numerical solutions for nonlinear progressive waves for a thin upper layer in the Boussinesq limit. Miles (1986) derived a second-order expansion for arbitrary depths and studied the evolution equations that govern Kelvin–Helmholtz waves in the parametric neighbourhood of the critical point. The work in this paper on flow of a gas over a thin liquid film closely follows the development of Saffman & Yuen (1982), who considered fluids of infinite extent and identified two different factors which limit the existence of steady gravity-wave solutions.

The first factor is what they called a 'geometrical limit', at which the wave profiles become unphysical as the wave height increases. Familiar examples of this are Stokes surface waves which develop a sharp corner at the crest and capillary waves for which the wave profile crosses itself at a critical height (Crapper 1957).

The second factor is what they called a 'dynamical limit'. It is encountered when the current velocity $U$ is increased, with the wave height kept fixed. For $U$ larger than a critical $U_c$, solutions at a given wave height cease to exist although the 'limiting wave' profile is smooth and exhibits no unphysical properties. For very small heights this dynamical limit is associated with the well-known Kelvin–Helmholtz instability; it may be interpreted as the non-existence of steady linear waves of a given wavelength when $U$ is sufficiently large. For finite-amplitude waves the critical current $U_c$ is a function of the wave height.

The effects of finite fluid depth and current velocity are investigated in the present

paper. Only the lower fluid depth $d_1$ is varied so the waves are functions of four parameters: wave amplitude $a$, fluid density ratio $r$, the relative velocity of the fluids $U$ and depth. For small-amplitude waves, algebraic expressions have been obtained for the leading-order nonlinear corrections. To obtain results for larger amplitudes, a new numerical method has been developed, which can handle fluids of arbitrary uniform depth and any density ratio.

The dynamical limit identified by Saffman & Yuen (1982) is shown to be influenced by changes in the fluid depth in an unexpected way. A very interesting result, brought out both by the analytical and the numerical calculation, is that for very shallow lower fluid (or equivalently long wavelengths) there are no steady wave solutions of any amplitude for current velocities higher than the critical $U_{cl}$ calculated from the linear Kelvin–Helmholtz analysis.

The question of the geometrical limit for waves of large height is also addressed. Extensive numerical calculations performed for the air–water system indicate that the location where the waves steepen with increasing amplitude depends strongly on the current velocity. These results imply that, if water waves are caused to break under the action of wind by reaching a limiting height, the point of breaking should depend on the wind velocity. This is an example of a situation where air, despite its very small density compared with that of water, has a profound effect on the behaviour of the system.

In §2 the mathematical formulation of the problem is given. The weakly nonlinear approximation is developeed in §3 and the numerical method in §4. Finally, the main results are presented in §5 are further discussed in §6.

## 2. Formulation of problem

Periodic gravity waves are considered at the interface between two fluids of uniform depth. The fluids have different densities and the upper is moving relative to the lower with a horizontal velocity $U$. They are taken to be incompressible and inviscid and the motion is assumed to be irrotational. Solutions are obtained for two-dimensional, periodic waves of wavelength $L$, which propagate without change of shape with phase speed $C$, in the direction of $U$. For the purpose of calculating steady waves, there is no loss of generality in taking $U$ parallel to $C$, as an arbitrary constant transverse velocity may be linearly superposed on the upper fluid's motion (Saffman & Yuen 1982). Properties of the lower fluid are denoted by 1 and those of the upper fluid, by 2. The two fluids are assumed to be stably stratified by gravity, so $\rho_2 < \rho_1$. Units of length, mass and time are chosen so that the wavelength $L = 2\pi$, the lower fluid density $\rho_1 = 1$ and the gravitational acceleration $g = 1$. Equivalently, all lengths are non-dimensionalized with the wavenumber $k$ and the velocities are Froude numbers using $k^{-1}$ as characteristic length.

The flow is sketched in figure 1. Rectangular coordinates $(x, y)$ are chosen such that the $x$-axis is horizontal and the $y$-axis is directed vertically upwards. The interface is located at $y = \eta$ and the bottom and top boundaries at $-d_1$ and $d_2$ respectively. The origin is chosen so that the mean elevation $\eta$ is zero. The reference frame is such that the fluid velocity averaged over one wave cycle (circulation), at any fixed depth within the lower fluid, is zero. For finite upper-fluid depth, the current velocity $U$ is defined similarly. It equals the fluid velocity averaged over one cycle, on any fixed height within the upper fluid. For an unbounded upper fluid, $U$ is simply the fluid velocity at infinity.

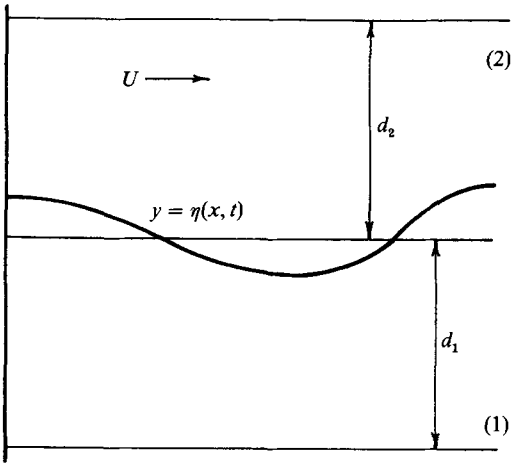


FIGURE 1. Sketch of flow system.

The kinematic boundary conditions, that require the interface to move with the vertical velocity of the fluids, are

$$\frac{\partial \eta}{\partial t}+\frac{\partial \phi_i}{\partial x}\frac{\partial \eta}{\partial x}=\frac{\partial \phi_i}{\partial y} \quad \text{at } y=\eta \quad (i=1,2). \tag{2.1}$$

For waves of permanent form

$$\frac{\partial \eta}{\partial t}=-C_{\mathrm{R}}\frac{\partial \eta}{\partial x}, \tag{2.2}$$

where $C_{\mathrm{R}}$ is the wave velocity in the reference frame used. If (2.2) is substituted into (2.1) it follows that

$$-C_{\mathrm{R}}\frac{\partial \eta}{\partial x}=\nabla\phi_i\cdot\boldsymbol{\alpha}, \tag{2.3}$$

where $\boldsymbol{\alpha}$ is the vector $(-\partial\eta/\partial x, 1)$ which is normal to the interface. The fluid velocity component normal to the interface is the dot product of the velocity potential gradient and the unit normal vector $\boldsymbol{n}$. If $\boldsymbol{\alpha}$ is written as the unit normal $\boldsymbol{n}$ times the magnitude of $\boldsymbol{\alpha}$ it follows from (2.3) that

$$-C_{\mathrm{R}}\frac{\partial \eta}{\partial x}=(\nabla\phi_i\cdot\boldsymbol{n})\left(1+\left(\frac{\partial \eta}{\partial x}\right)^2\right)^{\frac{1}{2}}, \tag{2.4}$$

or

$$\frac{\partial \phi_i}{\partial \boldsymbol{n}}=\nabla\phi_i\cdot\boldsymbol{n}=-C_{\mathrm{R}}\frac{\dfrac{\partial \eta}{\partial x}}{\left(1+\left(\dfrac{\partial \eta}{\partial x}\right)^2\right)^{\frac{1}{2}}}. \tag{2.5}$$

Equation (2.5) is the kinematic boundary condition used. For reasons that will become clearer with the development of the boundary integral calculation, the above

condition is applied to each fluid in a reference frame such that the fluid has circulation zero (or is at rest at infinity). Therefore,

$$\frac{\partial \phi_1}{\partial n} = -C \frac{\dfrac{\partial \eta}{\partial x}}{\left(1+\left(\dfrac{\partial \eta}{\partial x}\right)^2\right)^{\frac{1}{2}}} \quad \text{at } y = \eta, \tag{2.6}$$

$$\frac{\partial \phi_2}{\partial n} = -(U-C) \frac{\dfrac{\partial \eta}{\partial x}}{\left(1+\left(\dfrac{\partial \eta}{\partial x}\right)^2\right)^{\frac{1}{2}}} \quad \text{at } y = \eta. \tag{2.7}$$

A second rectangular coordinate system $(X, Y)$ is considered now, moving in the positive $x$-direction with the waves, at speed $C$. In this reference frame the motion is independent of time. The dynamic boundary condition, which is continuity of pressure at the interface, is applied in this coordinate system. Bernoulli's equation above and below the interface is used to obtain expressions for the pressure.

$$\frac{p_1}{\rho_1} = -\tfrac{1}{2}(\nabla \phi_1)^2 - gy + K_1, \quad \frac{p_2}{\rho_2} = -\tfrac{1}{2}(\nabla \phi_2)^2 - gy + K_2, \tag{2.8}$$

where $K_1, K_2$ are Bernoulli constants. Combining these equations on $y = \eta$ where $p_1 = p_2$,

$$\tfrac{1}{2}q_1^2 - \tfrac{1}{2}rq_2^2 + (1-r)g\eta + K = 0, \tag{2.9}$$

where

$$q_1^2 = (\nabla \phi_1)^2, \quad q_2^2 = (\nabla \phi_2)^2,$$
$$r = \rho_2/\rho_1, \quad K = rK_2 - K_1.$$

Equation (2.9) is the basis of the proposed numerical computation. For unbounded fluids the constant $K$ can be calculated in advance (Saffman & Yuen 1982) as

$$K = \tfrac{1}{2}r(C-U)^2 - \tfrac{1}{2}C^2. \tag{2.10}$$

For fluids of finite depth, however, $K$ is not known *a priori* and is treated as one more unknown.

## 3. Weakly nonlinear approximation

The properties of weakly nonlinear steady waves were obtained by using Whitham's averaged variational principle (see Whitham 1974, §16.6). The alternative of substituting Stokes expansions directly in the original set of equations and boundary conditions involves much lengthier algebra and was not attempted.

For irrotational interfacial waves with a current $U$ and lower and upper boundaries at $-d_1$ and $d_2$ respectively $(d_1 > 0, d_2 > 0)$, the averaged Lagrangian is given by

$$L = -\overline{\int_{-d_1}^{\eta} \left[\frac{\partial \phi_1}{\partial t} + \tfrac{1}{2}(\nabla \phi_1)^2 + gy\right] \mathrm{d}y} - \overline{\int_{\eta}^{d_2} \left[r\frac{\partial \phi_2}{\partial t} + \tfrac{1}{2}r(\nabla \phi_2)^2 + rgy\right] \mathrm{d}y} - L_0, \tag{3.1}$$

where the overbar denotes averaging over one cycle of the wave phase and

$$L_0 = -\int_{-d_1}^{\eta} gy \, \mathrm{d}y - \int_0^{d_2} (\tfrac{1}{2}rU^2 + rgy) \, \mathrm{d}y \tag{3.2}$$

is included only when one or both boundaries move to infinity, in order to ensure a convergent value for $L$. Note that in the present section the frame of reference is fixed

relative to the lower fluid and the units are arbitrary, so $k$ and $g$ appear in the equations.

Following Whitham (1974), the leading-order terms for the wave profile and the velocity potentials are substituted in the expressions for $L$.

$$\eta(w) = a\cos w + a_2\cos 2w, \tag{3.3}$$

$$\phi_1(x,y,t) = A_1(\mathrm{e}^{ky}+\mathrm{e}^{2kd_1}\,\mathrm{e}^{-ky})\sin w + \tfrac{1}{2}A_2(\mathrm{e}^{2ky}+\mathrm{e}^{4kd_1}\,\mathrm{e}^{-2ky})\sin 2w, \tag{3.4}$$

$$\phi_2(x,y,t) = Ux + B_1(\mathrm{e}^{ky}+\mathrm{e}^{2kd_2}\,\mathrm{e}^{-ky})\sin w + \tfrac{1}{2}B_2(\mathrm{e}^{2ky}+\mathrm{e}^{4kd_2}\,\mathrm{e}^{-2ky})\sin 2w, \tag{3.5}$$

where $w$ is the wave phase

$$w = kx - \omega t. \tag{3.6}$$

It is anticipated that $A_1$ and $B_1$ are $O(a)$ and $a_2, A_2$ and $B_2$ are $O(a^2)$, and terms up to $O(a^4)$ are retained in the expresion for $L$. Note that the $O(a^3)$ and $O(a^4)$ terms in the expansions (3.3)–(3.5) automatically disappear during the averaging procedure, so the expression for the Lagrangian $L$ is on the whole of accuracy $O(a^4)$. The coefficients $A_1$, $B_1$, $A_2$ and $B_2$ are eliminated by use of the equations

$$\partial L/\partial A_1 = \partial L/\partial B_1 = \partial L/\partial A_2 = \partial L/\partial B_2 = 0, \tag{3.7}$$

and after some algebra it is found that

$$\begin{aligned} L = {} & -\tfrac{1}{2}rU^2d_2 + \tfrac{1}{2}g(d_1^2 - rd_2^2) + \tfrac{1}{4}g(r-1)(a^2+a_2^2) + \tfrac{1}{4}ka^2\left(\lambda^2\frac{1+x}{1-x} + r\lambda'^2\frac{1+y}{1-y}\right) \\ & - \tfrac{1}{4}k^2a^2a_2\left[\lambda^2\frac{1+4x+x^2}{(1-x)^2} - r\lambda'^2\frac{1+4y+y^2}{(1-y)^2}\right] + \tfrac{1}{2}ka_2^2\left(\lambda^2\frac{1+x^2}{1-x^2} + r\lambda'^2\frac{1+y^2}{1-y^2}\right) \\ & + \tfrac{1}{4}k^3a^4\left\{\lambda^2\left(\frac{1+x}{1-x}\right)\left[\frac{x}{(1-x)^2} - \frac{1}{4}\right] + r\lambda'^2\left(\frac{1+y}{1-y}\right)\left[\frac{y}{(1-y)^2} - \frac{1}{4}\right]\right\}, \end{aligned} \tag{3.8}$$

where

$$x = \mathrm{e}^{-2kd_1}, \quad y = \mathrm{e}^{-2kd_2}, \tag{3.9}$$

$$\lambda = C_1 = \text{linear phase speed},$$

$$\lambda' = U - C_1,$$

and $\lambda, \lambda'$ are related by the linear dispersion relation

$$\lambda^2\frac{1+x}{1-x} + r\lambda'^2\frac{1+y}{1-y} = \frac{g}{k}(1-r). \tag{3.10}$$

The value of $a_2$ is found from $\partial L/\partial a_2 = 0$ and is substituted in (3.8). The dispersion relation for the weakly nonlinear wave then follows from $\partial L/\partial(a^2) = 0$:

$$\begin{aligned} & \frac{1+x}{1-x}C^2 + r\frac{1+y}{1-y}(U-C)^2 \\ & = \frac{g}{k}(1-r)\left[1 + \tfrac{1}{2}k^2a^2 - 2k^2a^2\frac{y}{(1-y)^2} + 2k^3a^2\frac{\lambda^2}{g(1-r)}\left(\frac{1+x}{1-x}\right)\left[\frac{y}{(1-y)^2} - \frac{x}{(1-x)^2}\right]\right. \\ & \left. + \tfrac{1}{2}k^2a^2\frac{\left\{\dfrac{k\lambda^2}{g(1-r)}\left[\dfrac{1+4x+x^2}{(1-x)^2} + \left(\dfrac{1+x}{1-x}\right)\left(\dfrac{1+4y+y^2}{1-y^2}\right)\right] - \left(\dfrac{1+4y+y^2}{1-y^2}\right)\right\}^2}{\left\{\left(\dfrac{1-y}{1+y}\right)^2 + \dfrac{2k\lambda^2}{g(1-r)}\left(\dfrac{1+x^2}{1-x^2} - \dfrac{1+x}{1-x}\dfrac{1+y^2}{(1+y)^2}\right)\right\}}\right], \end{aligned} \tag{3.11}$$

where $x, y$ are again given by (3.9). For fluids of infinite extent $d_1 \to +\infty, d_2 \to +\infty$ and $x = y = 0$. It can be verified that in this case (3.11) above agrees with that given by Saffman & Yuen (1982).

## 4. Numerical method

### 4.1. *Outline*

In the numerical method developed the wave is characterized by its phase velocity $C$ and the problem is solved in a coordinate system moving horizontally with velocity $C$. Equation (2.9) is applied at $N$ points along the interface. These equations together with the specification of the mean wave elevation $\eta = 0$ form an algebraic system of $N+1$ equations, with unknowns the profile elevations at the $N$ points and the combined Bernoulli constant $K$ (see equation (2.9)). The system is solved by a variation of Newton's method. At each iteration the fluids' velocities at the interface are calculated by applying a boundary integral method for the known boundary (the outcome of the last iteration) moving horizontally with the known velocity $C$. The matrix of partial derivatives is calculated numerically by perturbing each elevation by a small amount and computing the change in velocity at each point. It was found to be both efficient and time-saving to calculate the matrix once and use these values for all iterations. Owing to the approximation introduced by substituting integrals with linear sums, the set of equations is not satisfied exactly. Instead, the mean-square error is minimized over the $N$ points. This criterion works satisfactorily in the sense that it is easily driven to a minimum, which decreases by increasing the discretization $N$.

### 4.2. *Coordinate transformation*

For a periodic interface of given shape, moving horizontally with known phase velocity $C$, equations (2.6) and (2.7) give the normal component of the fluid velocity on the interface. To calculate the tangential velocity component (and therefore the velocity magnitudes $q_1, q_2$) a boundary integral method, developed by Longuet-Higgins & Cokelet (1976) and extended for finite depths by New, McIver & Peregrine (1985), is used.

Since the motion is periodic in $x$ with period $2\pi$, define for the lower fluid,

$$\zeta = r\,\mathrm{e}^{\mathrm{i}\theta} = \mathrm{e}^{-\mathrm{i}z} \quad (z = x + \mathrm{i}y). \tag{4.1}$$

Equation (4.1) maps one wavelength of the interface to the closed curve $C_1$ and the horizontal bottom $y = -d_1$ to a circle $C_2$ of radius $\mathrm{e}^{-d_1}$ (see figure 2). The $r$ and $\theta$ are polar coordinates in the $\zeta$-plane and from (4.1)

$$\left.\begin{aligned} r &= \mathrm{e}^{y} \quad \text{or } y = \ln r, \\ \theta &= -x \qquad x = -\theta. \end{aligned}\right\} \tag{4.2}$$

The treatment of the upper fluid differs only in that the transformation

$$\zeta = r\,\mathrm{e}^{\mathrm{i}\theta} = \mathrm{e}^{\mathrm{i}z} \quad (z = x + \mathrm{i}y), \tag{4.3}$$

is used, with,

$$\left.\begin{aligned} r &= \mathrm{e}^{-y} \quad \text{or } y = -\ln r, \\ \theta &= x \qquad x = \theta, \end{aligned}\right\} \tag{4.4}$$

so that the domain occupied by the upper fluid maps to a bounded region, as for the lower fluid.

If a fluid has a non-zero circulation $V$, then the expression for the velocity

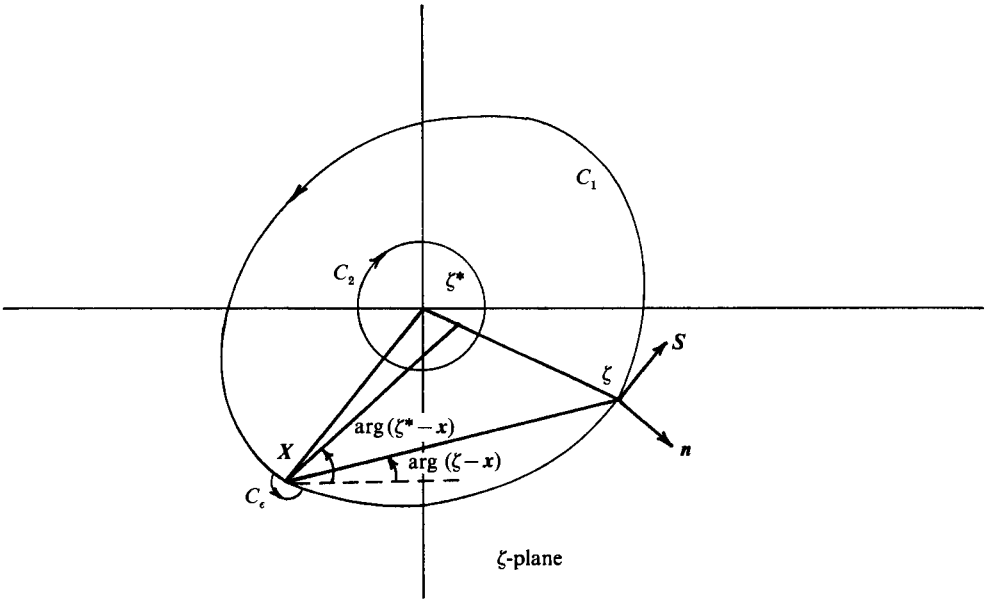


FIGURE 2. The transformed $\zeta$-plane, showing the construction of Green's function. $C_1$ represents one wavelength of the interface and $C_2$ is the bottom (or top) boundary.

potential will contain the term $Vx$ and therefore it will not be single-valued in the transformed coordinate system. This necessitates the definition of a branch-cut, making the computations much more complicated. By choosing (as was done in (2.6)–(2.7)) for each fluid a reference frame in which it has zero circulation, this difficulty is overcome.

According to the theory of complex functions, the velocity potential satisfies Laplace's equation in the transformed domain as it did in the original one. Therefore, to complete the new formulation, the kinematic boundary conditions need to be transformed to the $\zeta$-plane. If $\boldsymbol{N}$ and $\boldsymbol{n}$ are unit vectors normal to the boundary in the $(x, y)$ and $\zeta$-planes respectively, then it follows that (see figure 2):

$$\boldsymbol{N} = \frac{\left[\boldsymbol{i} - \left(\frac{\mathrm{d}y}{\mathrm{d}x}\right)\boldsymbol{j}\right]}{\left(1 + \left(\frac{\mathrm{d}y}{\mathrm{d}x}\right)^2\right)^{\frac{1}{2}}}, \quad \boldsymbol{n} = \frac{\left(\frac{\mathrm{d}Y}{\mathrm{d}\theta}\boldsymbol{i} - \frac{\mathrm{d}X}{\mathrm{d}\theta}\boldsymbol{j}\right)}{\left(\left(\frac{\mathrm{d}X}{\mathrm{d}\theta}\right)^2 + \left(\frac{\mathrm{d}Y}{\mathrm{d}\theta}\right)^2\right)^{\frac{1}{2}}} \tag{4.5}$$

where $X = r\cos\theta$, $Y = r\sin\theta$ and $X = X(\theta)$, $Y = Y(\theta)$ is a parametric description of the contour $C$ and

$$\frac{\mathrm{d}X}{\mathrm{d}\theta} = \cos\theta\frac{\mathrm{d}r}{\mathrm{d}\theta} - r\sin\theta, \quad \frac{\mathrm{d}Y}{\mathrm{d}\theta} = \sin\theta\frac{\mathrm{d}r}{\mathrm{d}\theta} + r\cos\theta. \tag{4.6}$$

Combining (4.5)–(4.6) with the transformation relations $r = \mathrm{e}^y, \theta = -x$ it follows that,

$$\frac{\partial\phi}{\partial n} = \frac{\left(-\frac{\mathrm{d}y}{\mathrm{d}x}\frac{\partial\phi}{\partial x} + \frac{\partial\phi}{\partial y}\right)}{\left(r^2 + \left(r\frac{\mathrm{d}y}{\mathrm{d}x}\right)^2\right)^{\frac{1}{2}}} = \frac{1}{r}\frac{\partial\phi}{\partial N}. \tag{4.7}$$

Therefore the correct kinematic boundary conditions for the transformed problem are, for the lower fluid,

$$\frac{\partial \phi_1}{\partial n} = -C\,\mathrm{e}^{-y}\frac{\left(\dfrac{\mathrm{d}y}{\mathrm{d}x}\right)}{\left(1+\left(\dfrac{\mathrm{d}y}{\mathrm{d}x}\right)^2\right)^{\frac{1}{2}}} \quad \text{at } y=\eta, \tag{4.8}$$

and for the upper,

$$\frac{\partial \phi_2}{\partial n} = -(U-C)\,\mathrm{e}^{y}\frac{\left(\dfrac{\mathrm{d}y}{\mathrm{d}x}\right)}{\left(1+\left(\dfrac{\mathrm{d}y}{\mathrm{d}x}\right)^2\right)^{\frac{1}{2}}} \quad \text{at } y=\eta. \tag{4.9}$$

### 4.3. *Formulation and solution of integral equation*

The problem of determining the tangential component of velocity at the boundary is equivalent to the Neumann problem of finding the value of a function $\phi$ whose normal gradient is given on a closed contour $C_1$. Suppose $\boldsymbol{x}$ is fixed at some point on the fluid boundary $C_1$, and $\boldsymbol{\xi}$ is allowed to vary along $C_1$. Let $(s, n)$ be tangential and normal coordinates at point $\boldsymbol{\xi}$ on the boundary (see figure 2). The integration of Green's third identity around the fluid boundary gives

$$\int_{C'}\left(G\frac{\partial \phi}{\partial n}-\phi\frac{\partial G}{\partial n}\right)\mathrm{d}s = 0. \tag{4.10}$$

Green's function, $G(\boldsymbol{x};\boldsymbol{\xi})$, is defined at all points in the fluid domain except $\boldsymbol{\xi}=\boldsymbol{x}$ and satisfies Laplace's equation. Contour $C'$ is the fluid boundary suitably indented to include a semicircular contour $C_\epsilon$ of vanishingly small radius at $\boldsymbol{x}$. Longuet-Higgins & Cokelet (1976), dealing with an unbounded fluid, used a simple logarithmic singularity

$$G(\boldsymbol{x};\boldsymbol{\xi}) = \frac{1}{2\pi}\ln|\boldsymbol{\xi}-\boldsymbol{x}|, \tag{4.11}$$

and derived an integral equation involving the tangential and normal derivatives of the velocity potential $\phi$, along the boundary. For finite fluid of depth $d$, the integration path in (4.10) has to include the bottom contour $C_2$, as well. New *et al.* (1985) used a Green's function involving an image singularity at $\boldsymbol{\xi}^* = \mathrm{e}^{-2d}\boldsymbol{\xi}/|\boldsymbol{\xi}|^2$ which is the geometrical reflection of $\boldsymbol{\xi}$ in the bottom contour $C_2$. The Green's function was thus given by

$$G(\boldsymbol{x};\boldsymbol{\xi}) = \frac{1}{2\pi}\ln R(\boldsymbol{x};\boldsymbol{\xi}), \quad R(\boldsymbol{x};\boldsymbol{\xi}) = |\boldsymbol{\xi}-\boldsymbol{x}|\,|\boldsymbol{\xi}^*-\boldsymbol{x}|. \tag{4.12}$$

The advantage of the above choice is that the normal derivative of $G$ is zero along $C_2$. Since, due to the no-penetration boundary condition, this is true for $\phi$ as well, the integration in (4.10) needs to be carried out only for the outer contour $C_1$. After some algebraic manipulations, (4.12) reduces to

$$\oint_{C_1}\ln R(\boldsymbol{x};\boldsymbol{\xi})\frac{\partial \phi}{\partial n}\mathrm{d}s = -\mathrm{P}\!\!\!\!\!\!\int \alpha(\boldsymbol{x};\boldsymbol{\xi})\frac{\partial \phi}{\partial s}\mathrm{d}s, \tag{4.13}$$

where, $\alpha(\boldsymbol{x};\boldsymbol{\xi}) = \arg(\boldsymbol{\xi}-\boldsymbol{x})-\arg(\boldsymbol{\xi}^*-\boldsymbol{x})$ and the integral on the right-hand side is principal in the sense that the contribution from $C_\epsilon$ is not included.

In the problem considered here, $\partial\phi/\partial n$ is known along the boundary from (2.6)–(2.7) and $\partial\phi/\partial s$ is computed by applying (4.13) once for the lower and once for the upper fluid. The left-hand side integral in (4.13) is calculated in exactly the same way as by Longuet-Higgins & Cokelet (1976). The right-hand side integral is approximated over a number of points $N$, by repeated application of Simpson's rule and the resulting system of linear equations is solved by direct Gaussian elimination. Next, the result is transformed to the original coordinate system. By an argument similar to the one presented for the kinematic boundary conditions (see equation (4.7))

$$\partial\phi/\partial S = r(\partial\phi/\partial s), \tag{4.14}$$

where $S$ is the arclength along the actual wave. Note that, to apply (2.9) which refers to a frame moving with the wave velocity $C$, the tangential component of the appropriate horizontal velocity needs to be subtracted from the above result. This is $C$ for the lower and $(C-U)$ for the upper fluid.

### 4.4. *Performance and accuracy*

The accuracy of the proposed numerical method was checked by calculating Stokes surface waves for various water depths. The Pade approximants calculation performed by Cokelet (1977) was duplicated and the results were compared. For a discretization of $N = 32$ points there was agreement to at least three decimal figures for waves as high as 90% of the limiting one. Increasing the number of points to 48 achieved the above accuracy for waves that are 94% of the highest. The agreement was further confirmed by comparing the wave profiles, which were visually indistinguishable. The accuracy of the numerical method was not appreciably affected by increased shallowness.

Interfacial waves between two stationary fluids with density ratio $r = 0.1$ have been calculated by Holyer (1979) using Pade approximants and by Saffman & Yuen (1982) and Meiron & Saffman (1983) numerically. Results by the present method agree to four decimal figures for waves with dimensionless heights up to 0.8. For higher waves there is a slight disagreement between the numbers reported by Saffman & Yuen and by Holyer. Results using the method just described are in closer agreement to those of Saffman & Yuen than to those of Holyer.

The conclusion from the above comparisons is that the proposed method is accurate for the calculation of highly nonlinear waves. The accuracy gradually deteriorates as the singular limiting wave is approached.

## 5. Results

### 5.1. *The critical current velocity*

It can be seen from the dispersion relation (3.11) that for linear waves ($a \to 0$) and given values of density ratio $r$, current velocity $U$ and fluids depth $d_1, d_2$, there are two solutions corresponding to the two roots of the quadratic equation for $C$. These are denoted by $C_+$ and $C_-$, where $C_+ > C_-$. For the linear case steady solutions cease to exist when $U$ exceeds a critical value $U_{c1}$ (the second subscript 1 standing for linear) given by

$$U_{c1} = \left\{\left(\frac{1-r}{r}\right)\frac{\left(\frac{1+x}{1-x}+r\frac{1+y}{1-y}\right)}{\left(\frac{1+x}{1-x}\right)\left(\frac{1+y}{1-y}\right)}\right\}^{\frac{1}{2}}, \tag{5.1}$$

and

$$C_+ = C_- = \frac{r\left(\frac{1+y}{1-y}\right)}{\left(\frac{1+x}{1-x}+r\frac{1+y}{1-y}\right)}U_{c1}. \tag{5.2}$$

As before, $x = e^{-2kd_1}$, $y = e^{-2kd_2}$ and the appropriate units are reintroduced to render $k = 1, g = 1$.

For finite amplitude waves ($a \neq 0$) these two solutions continue into two families of solutions $C_+(a)$ and $C_-(a)$. From the form of dispersion relation (3.11) for finite-amplitude waves it can be sen that there will again be a critical current $U_c$ beyond which steady solutions no longer exist. Saffman & Yuen (1982) calculated $U_c$, both analytically (second-order approximation) and numerically, for unbounded fluids. They were the first to note that the critical current velocity increases for increasing wave amplitude $a$, a result that can be viewed as a stabilization of parallel flows by waves. Thus, for a given value of $U > U_{c1}$, steady interfacial configurations exist on unbounded fluids only if there are waves with heights greater than some minimum.

A main focus of the present work was to determine the dependence of this phenomenon on the lower fluid depth. The motivation was to provide an understanding of interfacial waves for the flow of gas and liquid in a pipeline. For stratified flows, the liquid flowing along the bottom of the pipe is often shallow, with depth typically one order of magnitude smaller than the pipe diameter (Andritsos 1985). Situations in which both the liquid and the gas flow are shallow are also of interest in understanding the initiation of slug flow (Lin & Hanratty 1986).

The value of the critical current velocity $U_c$, correct to second order in the amplitude $a$, can be obtained by equating the two roots in (3.11)

$$U_{c2} = U_{c1}\left\{1+\tfrac{1}{2}a^2-2a^2\frac{r}{\left(\frac{1+x}{1-x}+r\right)}\frac{x}{(1-x)^2}+\tfrac{1}{2}a^2\frac{\left[\frac{r}{\left(\frac{1+x}{1-x}+r\right)}\left(1+\frac{1+4x+x^2}{1-x^2}\right)-1\right]^2}{\left[1+2\frac{r}{\left(\frac{1+x}{1-x}+r\right)}\left(\frac{1+x^2}{(1+x)^2}-1\right)\right]}\right\}^{\frac{1}{2}}, \tag{5.3}$$

where, as before, $x = e^{-2d_1}$ and the subscript 2 stands for second-order approximation. In the limit $d_1 \to +\infty$ the equation agrees with that given by Saffman & Yuen (1982). For the case of a liquid film of arbitrary depth considered in (5.3), $[(U_{c2}/U_{c1})^2-1]$ varies linearly with $a^2$ with the slope of the line varying with fluid depth. Figure 3 shows this slope, normalized with the deep-fluid slope, as a function of $e^{-kd_1}$ for three values of the density ratio ($r = 0.1, 0.5, 0.9$). It is evident that for gas–liquid systems ($r < 0.1$) there is not much change in the slope until $kd_1$ becomes very small (note that, for example, $e^{-kd_1} = 0.80$ corresponds to $d_1 = \frac{1}{28}L$). It is interesting, however, to note that there are regions where the slope is negative. In these regions an increase in the amplitude $a$ of steady waves gives rise to a decrease of critical velocity $U_{c2}$. This is just the opposite of what is found for unbounded fluids in that no steady wave solutions of a given wavelength exist for current velocities higher than the critical predicted from linear theory $U_{c1}$. Even for that velocity, the only steady wave is one of zero amplitude. Furthermore, for current velocities less than $U_{c1}$ the dynamical limit imposes a maximum allowable wave steepness $ka$. In this region and for current velocities close enough to the critical linear $U_{c1}$, large amplitude waves are

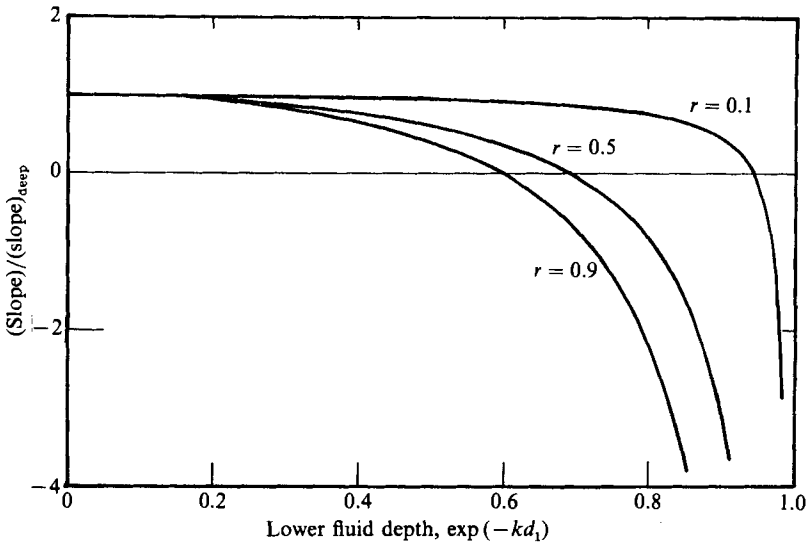


FIGURE 3. Slope of the $[U_c^2/U_{cl}^2 - 1]$ *vs.* $H^2$ line (normalized with deep fluid slope) versus depth. Weakly nonlinear approximation results for density ratios $r = 0.1, 0.5, 0.9$.

dynamically and not geometrically limited in steepness. It is noted that this observation is closely related to Miles' (1986) findings about the bifurcation associated with the critical point for the *K–H* instability, turning under some conditions from supercritical to subcritical.

The results of the numerical calculation of $U_c$ versus waveheight $H$ ($H = 2a$) for density ratio $r = 0.1$ are shown in figure 4 ($a$, $b$, $c$). The lower fluid depths are $e^{-d_1} = 0.25$, 0.60 and 0.80 respectively. The numerical results compare well with the weakly nonlinear approximation for intermediate to large depths. It is interesting to note that, at a fixed current speed, the weakly nonlinear theory overestimates the minimum wave height for a deep fluid but underestimates it for a shallow fluid. Larger deviations appear in the last figure, probably due to a more pronounced influence of the bottom boundary on the flow field.

The results of a numerical calculation of $U_c$ versus waveheight $H$ ($H = 2a$) for density ratio $r = 0.29$ and lower fluid depth $e^{-d_1} = 0.9048$ are shown in figure 5. At these conditions the second-order theory predicts that the critical velocity $U_c$ decreases with increasing amplitude. The numerical results indicate that, even at this very shallow depth, the fully nonlinear solution closely follows the weakly nonlinear result. Therefore, the unexpected effect of wave amplitude on $U_c$ for thin liquid layers found with second-order theory is real and not an artifact resulting from ignoring higher-order terms in the expansion.

### 5.2. *Geometrical limitation of the highest waves*

Holyer (1979) showed that, for waves at the interface between two stationary fluids, the slope eventually becomes infinite as the amplitude is increased. The location of this point of infinite slope depends on the density ratio of the two fluids and moves from the crest (a sharp corner) for free-surface waves, to the midpoint for fluids of almost equal densities (Boussinesq waves). Meiron & Saffman (1983) demonstrated numerically the existence of overhanging waves as steady solutions for two stationary fluids. They concluded that a geometrical limitation is associated with

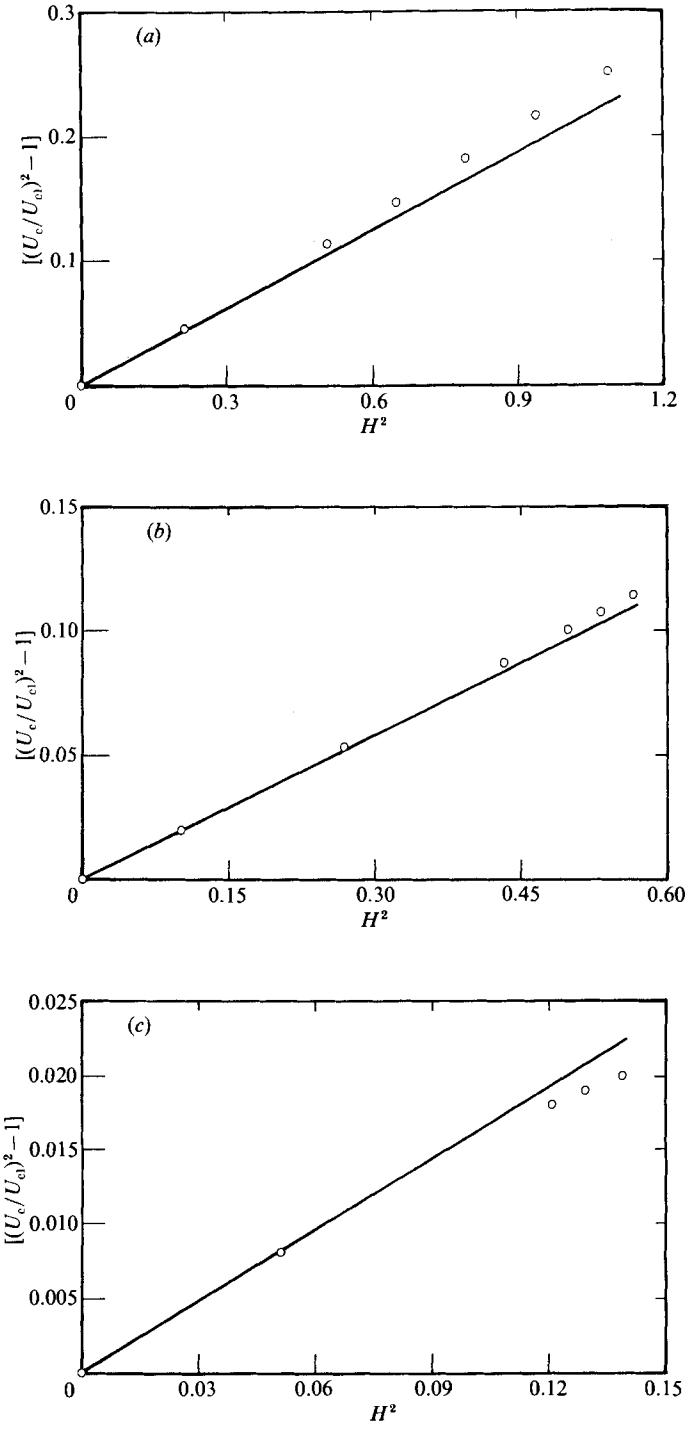


FIGURE 4. Critical current $U_c$ as a function of waveheight $H$, for density ratio $r = 0.1$ and $\exp(-d_1)$ (*a*) 0.25; (*b*) 0.60; (*c*) 0.80. Circles are numerical results using 48 points along one wavelength. Lines represent the weakly nonlinear approximation given by equation (5.3).

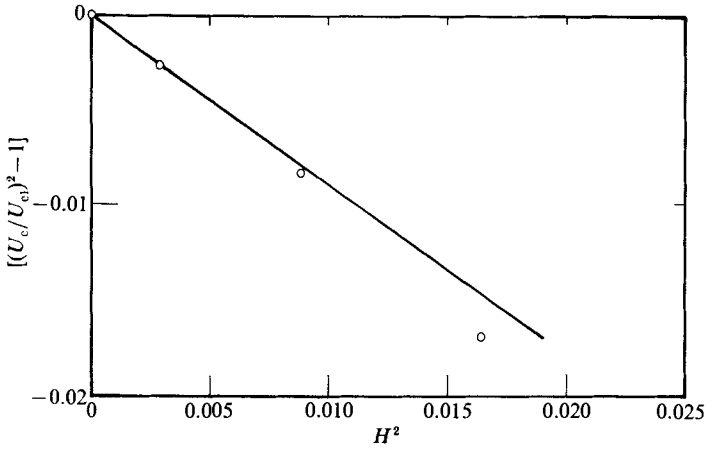


FIGURE 5. Critical current $U_c$ as a function of waveheight $H$, for density ratio $r = 0.9$ and $\exp(-d_1) = 0.9048$.

the surface crossing itself rather than with an infinite slope. Saffman & Yuen (1982) speculated that a similar geometrical limitation would exist for fluids in relative motion and that the region of singularity would be close to the crest for $C_+$ and close to the trough for $C_-$ waves.

The numerical method presented in this paper cannot, in its present form, handle overhanging waves. Therefore it was used only to detect the approach to a wave with an inifinite slope in its profile. When a vertical slope first develops at a point in the profile, the $x$-velocity component there will equal the phase speed of the wave and will be the maximum along the profile (the profile of an overhanging wave includes fluid particles moving horizontally faster than the wave). Therefore, the horizontal velocity component of the lower fluid particles along the interface were calculated. A maximum develops as the amplitude of the wave increases and its position indicates the point where the infinite slope first develops. It is interesting to note that this method works for very small density ratios, for which the infinite slope and the accompanying overhanging region occur in such a small scale that prohibitively high resolution would be required if calculated wave profiles were used to determine geometrically limiting waves.

Results for air–water $C_+$ waves are presented ($r = 0.0013$), because of their frequent occurrence in practice. Figure 6(*a–d*) shows the horizontal velocity component of the lower fluid particles along the interface. The depth is $e^{-d_1} = 0.25$ and different curves on each figure correspond to increasing wave heights. The current velocity $U$ is 10, 20, 25, and 30 in (*a*), (*b*), (*c*) and (*d*) respectively. It is noted that a large region of almost constant horizontal velocity exists near the crest for large amplitude waves. A maximum in the $x$-velocity appears in each plot if the amplitude of the wave is large enough. The position of this maximum is about $\frac{2}{48}L$, $\frac{7}{48}L$, $\frac{10}{48}L$ and $\frac{15}{48}L$ away from the crest for current velocities $U = 10$, 20, 25 and 30. Similar calculations for $e^{-d_1} = 0.60$ indicate that the position of the maximum does not depend on the water depth.

The profiles of some high waves for the above current velocities are shown in figure 7. The beginning of the high slope region, which moves away from the crest as the current velocity $U$ increases, is at the location of maximum horizontal velocity. The overall shape of the waves is also strongly affected by $U$. For low current velocities

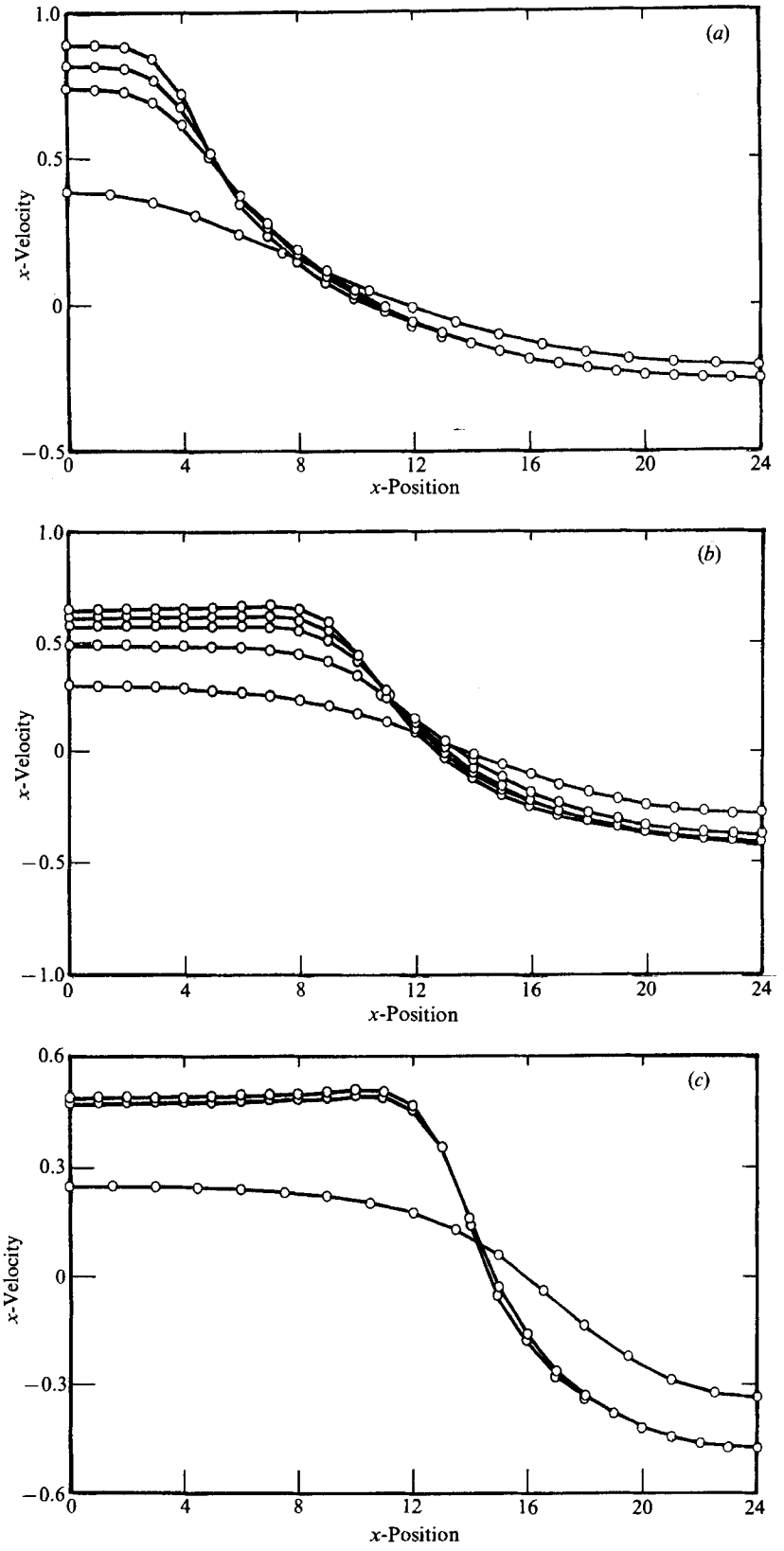


FIGURE 6(*a–c*). For caption see facing page.

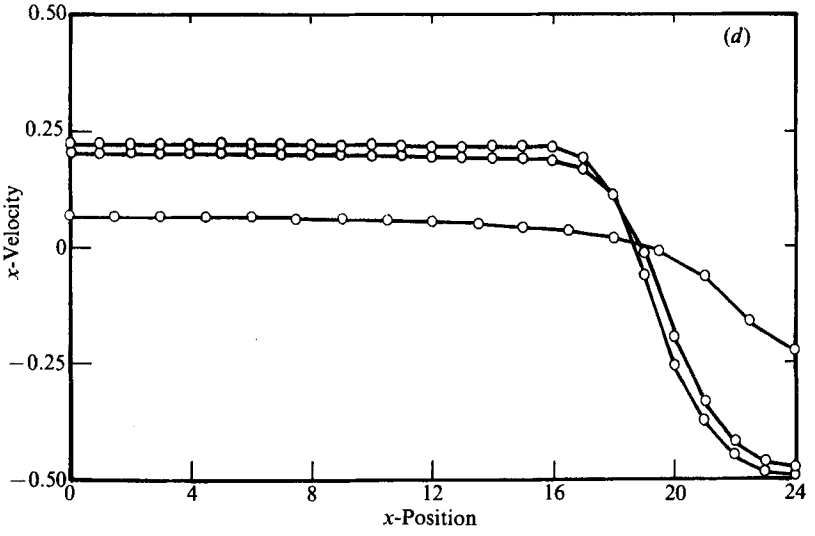


FIGURE 6. The $x$-velocity component of water particles versus position along one wavelength of air–water interface. Exponential depth $\exp(-d) = 0.25$ and current velocities $U$, (*a*) 10; (*b*) 20; (*c*) 25; (*d*) 30. The wave amplitudes are: (*a*) 0.289, 0.476, 0.511, 0.543; (*b*) 0.386, 0.581, 0.656, 0.687, 0.716; (*c*) 0.486, 0.750, 0.764; (*d*) 0.458, 0.658, 0.685 respectively.

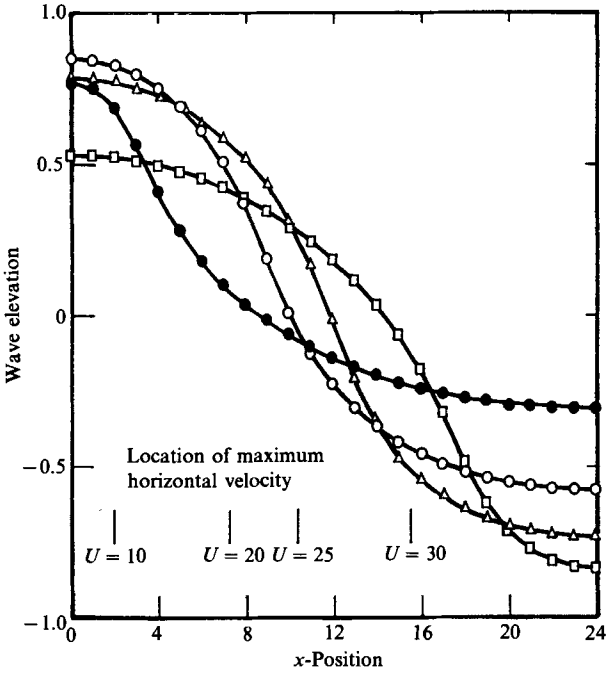


FIGURE 7. Profiles of high air–water waves for current velocities, ●, $U = 10$; ○, $U = 20$; △, $U = 25$; □, $U = 30$. The lines at the bottom represent the locations of maximum horizontal velocity from figure 6.

they are peaked at the crest, as observed for the free-surface waves of Stokes. As $U$ increases, however, the crest flattens and the trough becomes progressively sharper. This change agrees with what has been observed experimentally (Wallis & Dobson 1973).

## 6. Discussion

### 6.1. *Outline of contibutions*

A new numerical method for calculating periodic, interfacial, gravity waves has been developed. Its main advantages are that it is accurate for very shallow layers, for a wide range of current velocities and for fluids with any density ratio, thus enabling the investigation of the practically important case of air–water waves. Its main disadvantage is that it cannot handle overhanging waves and, therefore, cannot be used to calculate the geometrically limiting highest wave. However this does not seem to be a fundamental limitation since the boundary integral calculation is known to work with overhanging profiles. A modification of the iteration procedure is needed to take into account the possibility of a multiple-valued profile.

This numerical method and a weakly nonlinear approximation were used to obtain new unexpected results on the effect of the depth of the lower fluid on the dynamical limit to the existence of progressive waves of permanent form and on the effect of current velocity on the shape and limiting form of very high interfacial waves.

### 6.2. *Effect of fluid depth on the dynamical limit*

The increase in the critical current velocity with increasing wave amplitude, observed by Saffman & Yuen (1982) for unbounded fluids, is shown to become progressively less pronounced with decreasing depth. This effect is most evident for large values of density ratio. Furthermore, for small enough values of $kd_1$ the effect of increasing wave amplitude is just the opposite of what is observed for unbounded fluids; the critical velocity $U_c$ decreases with increasing amplitude and there are no steady wave solutions of given wavelength for current velocities larger than the critical predicted from linear theory.

These results are summarized in figure 8 which shows the variation of $[(U_{c2}/U_{c1})^2-1]$ with wave steepness $k^2a^2$ for two representative cases, one with positive and one with negative slope. Steady wave solutions exist in the region between the negative $y$-axis and the 'dynamical limit' line. The solution domain is also bounded to the right by the 'geometrical limit' which is not shown in the graph. It is evident that for a positive slope the restriction imposed by the dynamical limit is a minimum wave steepness when $U > U_{c1}$. With a negative slope there are no steady solutions for $U > U_{c1}$ and the restriction is a maximum steepness for $U < U_{c1}$.

Thus, for deep fluids, unstable $K$–$H$ disturbances are expected to grow into finite-amplitude waves. If interfacial waves generated by a different mechanism already exist, they are expected to steepen in accordance with the behaviour of the steady, periodic wave solutions. For a shallow enough lower fluid however, weakly nonlinear theory predicts that the inertia of the fluids and the gravity force cannot balance for any amplitude, for current velocities higher than the critical linear $U_{c1}$. For such current velocities, gravity waves with wavelengths longer than a given value should not be observed.

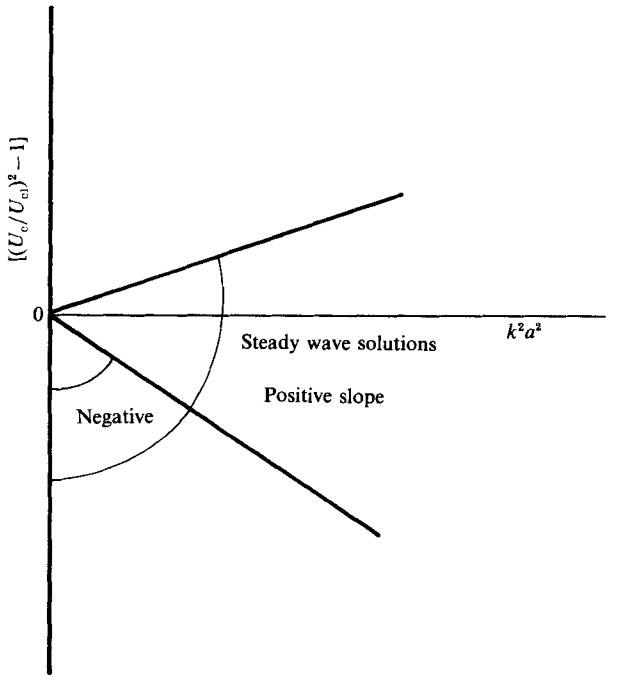


FIGURE 8. Critical current $U_{c2}$ as a function of the wave steepnes $ka$ for two representative cases. Steady wave solutions exist in the region between the negative $y$-axis and the 'dynamical limit' line.

### 6.3. *Effect of current velocity on the geometric limit*

Holyer (1979) calculated that, for the stagnant air–water system, the vertical tangent in the profile appears at a distance closer than $\frac{1}{100}L$ from the crest. Saffman & Yuen (1982) noted that, for small current velocities, there exists a special class of solutions with waves whose phase velocities equal $U$. They are transformations of the Stokes (1847) surface waves for $C_+ = U = (1-r)^{\frac{1}{2}}C_S(H)$, with $C_S(H)$ being the phase speed of the Stokes wave for a given height $H$. These waves are known to be geometrically limited, right on the crest, by the formation of a sharp corner for $H = 0.892$.

However, the results of the present work indicate that the location in the profile where a vertical tangent appears moves away from the crest and approaches the trough for high current velocities. An explanation that reconciles the above results is that, as the current velocity increases from zero, the region of singularity in the wave profile first moves towards the crest. For some current velocity it is located right on the crest, where it degenerates to a sharp corner. As $U$ is increased further the region of singularity moves away from the crest, approaching the trough as $U$ exceeds the linear critical value $U_{c1}$.

This phenomenon might have interesting implications for the breaking of water waves under the action of wind. For the air–water system and small current velocities the region of singularity in the wave profile remains very close to the crest. As can be seen in figure 7, for a current velocity as high as 10 the wave profile does not look very different from a surface wave and therefore the inferences made from classical steady-wave theory about breaking originating at the crest, still hold. For high current velocities, however, both the point of breaking and the shape of the wave change drastically and it seems reasonable to argue that a different breaking

mechanism might be involved. A conjecture is that a very small-scale overturning motion occurs, followed by the formation of a turbulent layer of foaming water at the location of the vertical tangent in the forward face of the wave. However, this remains to be investigated.

This work was supported by the National Science Foundation through Grant NSF CBT 88-00980 and by the Shell Companies Foundation.

## REFERENCES

ANDRITSOS, N. 1985 Effect of pipe diameter and liquid viscosity on horizontal stratified flow. PhD thesis, Dept. of Chem. Engng, University of Illinois at Urbana-Champaign.

COKELET, E. D. 1977 Steep gravity waves in water of arbitrary uniform depth. *Phil. Trans. R. Soc. Lond.* A **286**, 183.

CRAPPER, G. D. 1957 An exact solution for progressive capillary waves of arbitrary amplitude. *J. Fluid Mech.* **2**, 532.

DRAZIN, P. G. 1970 Kelvin–Helmholtz instability of finite amplitude. *J. Fluid Mech.* **42**, 321.

HOLYER, J. Y. 1979 Large amplitude progressive interfacial waves. *J. Fluid Mech.* **93**, 433.

LIN, P. Y. & HANRATTY, T. J. 1986 Prediction of the initiation of slugs with linear stability theory. *Intl J. Multiphase Flow* **12**, 79.

LONGUET-HIGGINS, M. S. & COKELET, E. D. 1976 The deformation of steep surface waves on water. I. A numerical method of computation. *Proc. R. Soc. Lond.* A **350**, 1.

MASLOWE, S. A. & KELLY, R. E. 1970 Finite amplitude oscillations in a Kelvin–Helmholtz flow. *Intl J. Non-Linear Mech.* **5**, 427.

MEIRON, D. J. & SAFFMAN, P. G. 1983 Overhanging gravity waves of large amplitude. *J. Fluid Mech.* **129**, 213.

MILES, J. W. 1986 Weakly nonlinear Kelvin–Helmholtz waves. *J. Fluid Mech.* **172**, 513.

NAYFEH, A. H. & SARIC, W. S. 1972 Nonlinear waves in Kelvin–Helmholtz flow. *J. Fluid Mech.* **55**, 311.

NEW, A. L., MCIVER, P. & PEREGRINE, D. H. 1985 Computations of overturning waves. *J. Fluid Mech.* **150**, 233.

PULLIN, D. I. & GRIMSHAW, R. H. J. 1983*a* Nonlinear interfacial progressive waves near a boundary in a Boussinesq fluid. *Phys. Fluids* **26** (4), 897.

PULLIN, D. I. & GRIMSHAW, R. H. J. 1983*b* Interfacial progressive gravity waves in a two-layer shear flow. *Phys. Fluids* **26**, 1731.

SAFFMAN, P. G. & YUEN, H. C. 1982 Finite-amplitude interfacial waves in the presence of a current. *J. Fluid Mech.* **123**, 459.

STOKES, G. G. 1847 On the theory of oscillatory waves. *Trans. Camb. Phil. Soc.* **8**, 441.

TSUJI, Y. & NAGATA, Y. 1973 Stokes expansion of internal deep water waves to the fifth order. *J. Ocean. Soc. Japan* **29**, 61.

WALLIS, G. B. & DOBSON, J. E. 1973 The onset of slugging in horizontal stratified air–water flow. *Intl J. Multiphase Flow* **1**, 173.

WEISSMAN, M. A. 1979 Nonlinear wave packets in the Kelvin–Helmholtz instability. *Phil. Trans. R. Soc. Lond.* A **290**, 639.

WHITHAM, G. B. 1974 *Linear and Nonlinear Waves*. Wiley-Interscience.